Applied Catalysis A: General 528 (2016) 168–174

Contents lists available at ScienceDirect

Applied Catalysis A: General

journal homepage: www.elsevier.com/locate/apcata

Highly dispersed Pd/AlPO-5 catalyst for catalytic hydrogenation of 2-ethylanthraquinone

Xiaotong Li[a,b,c], Hongjiu Su[a,b,*], Dawei Li[a,b,c], Haijun Chen[a,b], Xiaoye Yang[a,b], Shudong Wang[a,b,*]

[a] Dalian Institute of Chemical Physics, Chinese Academy of Sciences, Dalian 116023, Liaoning, China
[b] Dalian National Laboratory for Clean Energy, Dalian 116023, Liaoning, China
[c] University of Chinese Academy of Sciences, Beijing 100039, China

ARTICLE INFO

Article history:
Received 3 June 2016
Received in revised form
28 September 2016
Accepted 6 October 2016
Available online 13 October 2016

Keywords:
Pd catalyst
Metal-support interaction
Anthraquinone
Dispersion

ABSTRACT

Highly dispersed Pd/AlPO-5 catalyst was prepared and tested in the hydrogenation of 2-ethylanthraquinone. Characterization results suggested that the abundant surface P-OH groups of AlPO-5 zeolite substituted NH_3 ligands of $[Pd(NH_3)_4]^{2+}$ precursor to form $[Pd(NH_3)_3(POH)]^{2+}$. After calcination, the latter formed Pd-O-P interfacial linkage between Pd nanoparticles and AlPO-5, benefiting the suppression of Pd sintering. SiO_2 and SiO_2-AlPO-5 composite were used as supports for comparison. Catalyst supported on SiO_2-AlPO-5 composite (25 wt% AlPO-5) exhibited improved catalytic activity and stability in consideration of reactant activation as well as the mass transfer of reactant molecules, which is expected to decrease precious metal loading in industrial application.

© 2016 Elsevier B.V. All rights reserved.

1. Introduction

Metal nanoparticles (NPs) dispersion is one of the most important issues of heterogeneous catalyst. It has been reported that the strong interaction of metal NPs and oxide support can alter the electronic properties of the metal, influencing NPs morphology and dispersion [1]. Several attempts have involved the use of metal-support interactions to suppress NPs sintering. The strong metal support interaction was first found on reductive oxide supports such as CeO_2, TiO_2, V_2O_3, etc [2–5]. For example, the Pt-O-Ce bond was found to act as an anchor and inhibited the sintering of Pt NPs on CeO_2 under oxidative atmosphere [6]. Recently, a nonoxide support (phosphate hydroxyapatite) has been found to exhibit strong anti-sintering property due to strong metal-support interaction [7]. Besides, Machida et al. reported $AlPO_4$ supported Rh catalysts having high Rh dispersion due to the sintering suppression of Rh-O-P linkage between Rh nanoparticles and $AlPO_4$ support [8,9].

Environmentally friendly oxidant hydrogen peroxide is manufactured almost exclusively by the anthraquinone (AQ) process [10–12]. As shown in Scheme 1, the cyclic reaction starts with 2-ethylanthraquinone (eAQ) hydrogenation to yield 2-ethylanthrahydroquinone ($eAQH_2$) in the presence of Pd catalyst under hydrogen atmosphere then followed by autoxidation of $eAQH_2$ to yield H_2O_2 and eAQ simultaneously. Interfacial mass transfer is the limited step of eAQ hydrogenation. It has been reported that catalyst with higher Pd dispersion can improve hydrogenation efficiency effectively [13]. However, the reaction network of eAQ hydrogenation consist of various consecutive and competitive reactions, which produces various by-products such as tetrahydro-2-ethylanthrahydroquinone (H_4eAQH_2), octahydro-2-ethylanthrahydroquinone (H_8eAQH_2), 2-ethylanthrone (eAN) and tetrahydro-2-ethylanthrone (H_4eAN) (Scheme 1) [13,14]. Deep hydrogenation of $eAQH_2$ is inevitable. Among all the degradations, H_4eAQH_2 can produce H_2O_2 during the cyclic hydrogenation and oxidation process, hence, the AQ and tetrahydro-2-ethylanthraquinone (H_4eAQ) are both considered as active anthraquinone. 2-ethyloxoanthrone (OXO), the precursor of eAN and H_4eAN, is generated by the tautomerization of $eAQH_2$ during hydrogenation. The formation of OXO form is favoured in acidic conditions due to the tautomerization equilibrium [15,16]. OXO appears in the reaction mixture at the same time with $eAQH_2$ under hydrogen atmosphere. In air atmosphere, OXO isomerizes to the $eAQH_2$, however, the isomerization rate is quite slow.

Alumina is a widely-used support in the hydrogenation of 2-ethylanthraquinone, but previous researches have shown the

* Corresponding authors at: Dalian Institute of Chemical Physics, Chinese Academy of Sciences, Dalian 116023, Liaoning, China.
E-mail addresses: suhj@dicp.ac.cn (H. Su), wangsd@dicp.ac.cn (S. Wang).

http://dx.doi.org/10.1016/j.apcata.2016.10.007
0926-860X/© 2016 Elsevier B.V. All rights reserved.

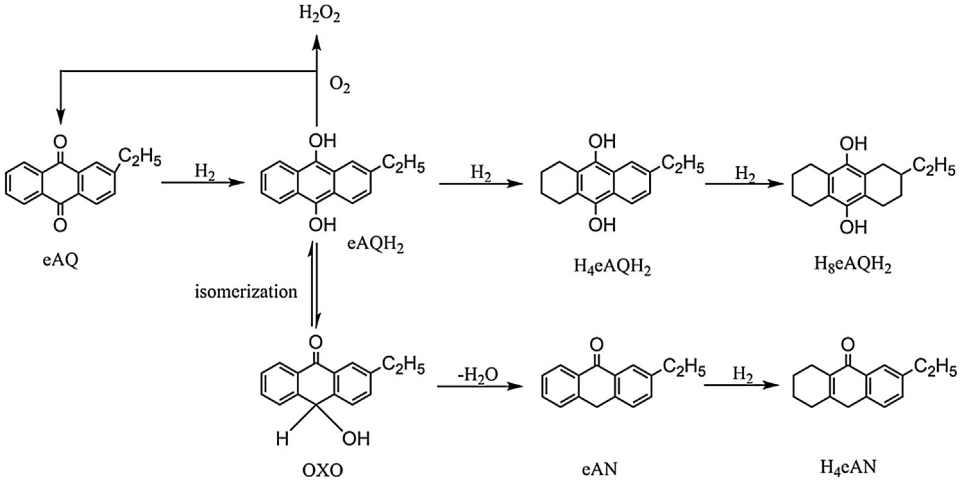

Scheme 1. Reaction network of the hydrogenation of 2-ethylanthraquinone.

support acidity leads to the increasing production of by-products [17–19]. Several methods have been proposed to avoid the negative effect of its acidity, such as support modification with Na_2SiO_3, NaH_2PO_4 and some alkali metals [20–22]. Moreover, silica is an excellent alternate for alumina due to its very weak acidity, but it shows poor resistance to metal sintering attributed to the relative weak interaction with metal nanoparticles [21,23]. A sintering resistant support with weak acidity is in demand.

With regular pore structure and good thermal stability, some zeolites are used as catalyst supports [24,25]. In contrast to the aluminosilicate zeolites, AlPO-n have strictly alternated Al and P on the tetrahedral nodes, which yield charge neutral framework. Since the lattice is overall charge neutral, aluminum phosphate does not possess the ion exchange ability or strong acidity [26]. In this work, Pd/AlPO-5 catalyst was prepared by impregnation method and tested in the liquid phase hydrogenation of eAQ. Given reactant molecular size, the microporous structure of AlPO-5 is unable to meet the mass transferring demand of the reactant and product molecules [26]. Hence, Pd catalysts with SiO_2-AlPO-5 composed support were also prepared and tested.

2. Experimental section

2.1. Preparation of the catalysts

2.1.1. Preparation of AlPO-5

The molar ratio of the starting gels were 1.2 TEA: 1 Al_2O_3: 1 P_2O_5: 50 H_2O. The gels were prepared by adding pseudoboehmite (Catapal C, Sasol) to a solution of phosphoric acid (Sinopharm Chemical reagent Co.) and stirred for 3 h. Then, tetraethylamine (TEA, Sinopharm Chemical reagent Co.) was added to the mixtures and stirred for 24 h. The resulting gels were introduced into teflon-lined, stainless steel autoclaves and heated at 200 °C for 36 h. After hydrothermal treatment, the formed zeolite was separated from the mother liquor, rinsed repeatedly with distilled water and dried. The dried zeolite was finally calcined at 600 °C for 6 h. N_2 isotherms and XRD patterns of calcined zeolite are shown in Figs. S1 and S2.

2.1.2. Preparation of composite support

SiO_2 (Haiyang Co. Qingdao) and AlPO-5 was milled and sieved to by a 200 mesh sieve, then mixed proportionally with silica sol (Ludox HS-30) and water. Then the mixture was dried at 100 °C, crushed and sieved (40–60 mesh). The pure AlPO-5 support was prepared by powder press method. The pressure of tablet press was 10 MPa. Obtained AlPO-5 tablets were crushed and sieved (40–60 mesh) to prepare pure AlPO-5 support.

2.1.3. Preparation of the catalysts

2 g prepared support was impregnated in 4 mL $Pd(NH_3)_4(NO_3)_2$ aqueous solution (1.25 g·L^{-1}, calculated by Pd mass) for 2 h, followed by drying and calcination at 400 °C for 2 h. Before reaction, the catalyst was reduced by H_2 at 120 °C for 2 h.

2.2. Characterization of the catalysts

Nitrogen physisorption was carried out to characterize specific surface areas and porosity of samples at liquid N_2 temperature in a Quantachrome NOVA 2200e instrument. The specific surface area and pore size distribution were determined by using the BET and the DFT method, respectively. Prior to analysis, the samples were degassed under vacuum condition at 200 °C for at least 2 h.

The transmission electron microscopy (TEM) measurement was carried out with a JEOL JEM-2000 EX equipment operated at an accelerating voltage of 120 kV. Before analysis, the catalyst was reduced in H_2/Ar at 120 °C for 1 h. The Pd loading was determined by an inductively coupled plasma-atomic emission spectroscopy (ICP-AES). The dispersion of palladium was measured through CO chemisorptions experiments on a Quantachrome CHEMBET Pulsar adsorption instrument. Before analysis, the catalyst was reduced in H_2/Ar at 120 °C for 1 h. The adsorption measurements were performed 45 °C in a He flow.

UV–vis spectra were recorded on a Cary 5000 Varian spectrophotometer in diffuse reflectance cell. The effluent was analyzed using a TOF-MS 500 mass spectrometer made by Dalian Institute of Chemical Physics.

In situ DRIFT spectra were recorded in the OH stretching frequency region using a Thermo Nicolet 6700 spectrometer equipped with a temperature-controllable diffuse reflectance reaction cell. The powder samples were placed in a crucible inside the cell before they were heated at increasing temperatures under He flow, which removed any adsorbed water. Pd/AlPO-5 samples that displayed different Pd loadings were pretreated using He flow at elevated temperatures for 1 h before the measurements were taken.

The H_2 temperature programmed reduction (H_2-TPR) experiments were performed on a flow system at a Quantachrome CHEMBET3000 adsorption instrument equipped with a TCD detector. Prior to reduction, catalyst samples were dried in an argon flow at 150 °C for 1 h. Then the sample was reduced in a 10 vol.% H_2/Ar flow system at a rate of 10 °C min^{-1} from −70 to 250 °C.

X-ray photoelectron spectra were acquired on a Thermo ESCALAB 250Xi XPS system using an Al*Kα* X-ray anode at a base pressure of about 1.7×10^{-10} mbar. Energies were calibrated using the C 1 s peak (284.6 eV). The catalyst samples were pre-reduced ex-situ under flow of H_2 (40 mL min^{-1}) at 70 °C for 1 h, followed by cooling under Ar atmosphere. The reduced samples were transferred into the XPS cell under Ar atmosphere to avoid exposure to air.

2.3. Test of catalyst performance

The activity test was carried out in a stainless steel trickle bed reactor at 40 °C with 1 g catalyst. The working solution was prepared by dissolving 12 g of solid eAQ (98%, global fine chemical Co. Yixing) in 100 mL of a mixed solvent of trioctyl phosphate (98%, nature chemical Co. Hangzhou) and C_9–C_{10} aromatic hydrocarbon (99%, Zhongke group, Shenyang) with the volume ratio of 1:3. The gas volumetric flow rate was set at 3 mL min^{-1}. By the sampling time, 5 mL catalyst-free hydrogenation products were oxidized with air at room temperature for 30 min. H_2O_2 was then extracted with deionized water to obtain a solution of H_2O_2. The content of H_2O_2 was analyzed by titration with $KMnO_4$ solution. Besides, the hydrogenation products were also analyzed by high performance liquid chromatography (HPLC) with Agilent 1100, equipped with a column of Kromasil® C18(5 μ, 150 × 4.6 mm), the mobile phase was the mixture of methanol and water with a ratio of 3:1.

The catalyst activity and selectivity are expressed by the following simplified equations:

$$B = \frac{5c_{KMnO_4} \times V_{KMnO_4} \times M_{H_2O_2}}{2V}$$

$$S = \frac{n_{(eAQ)} + n_{(H_4eAQ)}}{n_{0(eAQ)}} \times 100$$

where B is the hydrogenation efficiency (g·L^{-1}), C_{KMnO4} is the $KMnO_4$ solution concentration (mol·L^{-1}), V_{KMnO4} is the $KMnO_4$ solution volume (mL) and V is the H_2O_2 solution volume (mL), respectively. As the Pd loading of each catalyst is slightly different, the hydrogen efficiencies are normalized. S is the selectivity toward active quinones (eAQ and H_4eAQ), n_0 and n are the molar content of components in the initial working solution and in the accumulated re-oxidized solution, respectively.

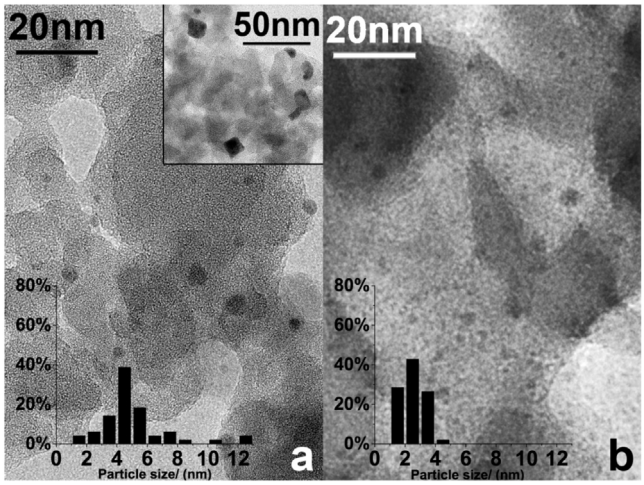

Fig. 1. TEM images of catalysts. (a) Pd/SiO_2; (b) Pd/AlPO-5.

3. Result and discussion

3.1. Characterization of the Pd/AlPO-5 and Pd/SiO_2 catalysts

N_2 adsorption was used to characterize the pore structure of two catalysts. From Table 1 and Fig. S3, it can be seen that Pd/AlPO-5 catalyst has narrow distributed microporous structure, while Pd/SiO_2 catalyst possesses regular mesoporous pore structure. The specific surface area and pore volume of Pd/AlPO-5 catalyst are lower than that of Pd/SiO_2 catalyst.

The TEM images of catalysts and the distribution of Pd particle size are shown in Fig. 1. Pd grains distributed on AlPO-5 support have average size of 2.6 ± 0.6 nm. The Pd dispersion measured by CO chemisorption is 34.6%. The Pd/SiO_2 achieves an average Pd particle size of 5.1 ± 1.5 nm. However, its Pd dispersion is 11. 1% due to the formation of large Pd aggregates (Fig. 1a, inset). The difference of Pd particle dispersion indicates that AlPO-5 support suppresses the Pd sintering effectively.

In order to understand the sintering suppression effect, the impregnation process was studied by UV–vis spectrophotometer and time of flight mass spectrometer (TOF-MS). Before impregnation, the $Pd(NH_3)_4(NO_3)_2$ solution was almost colorless owing to its low concentration with a pH of 9.5. After impregnation the colors of AlPO-5 support and its impregnation solution change to yellow while the colors of SiO_2 support and its impregnation

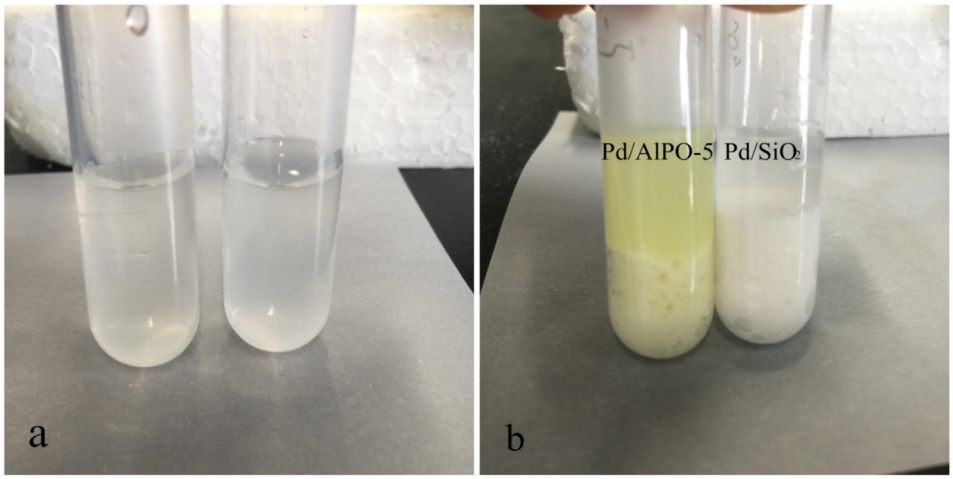

Fig. 2. (a) Photo of $Pd(NH_3)_4(NO_3)_2$ solution before impregnation; (b) after impregnation; Pd-/AlPO-5 (left), Pd/SiO_2 (right).

Table 1
Properties of catalysts.

Sample	AlPO-5 content (wt.%)	Pd loading[a] (wt.%)	Specific surface area[b] ($m^2 \cdot g^{-1}$)	Pore volume ($mL \cdot g^{-1}$)	Dispersion[c] (%)
Pd/A-0 (Pd/SiO_2)	0	0.24	231.1	0.86	11.1
Pd/A-25	25	0.26	178.7	0.43	25.3
Pd/A-50	50	0.25	165.2	0.38	30.9
Pd/A-75	75	0.24	157.5	0.27	33.9
Pd/A-100 (Pd/AlPO-5)	100	0.26	170.7	0.16	34.6
1%Pd/AlPO-5	100	1.01	156.5	0.16	27.0
3%Pd/AlPO-5	100	2.56	147.0	0.15	15.6

[a] Measured by ICP-AES.
[b] Calculated by BET method.
[c] Measured by CO pulsar chemisorption.

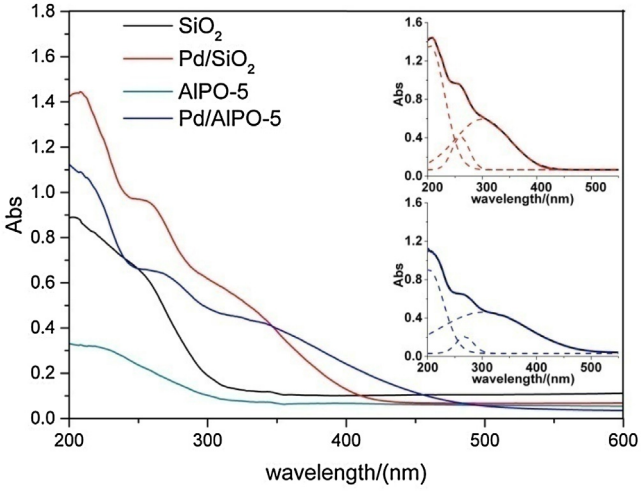

Fig. 3. UV–vis spectra of catalysts before and after impregnation.

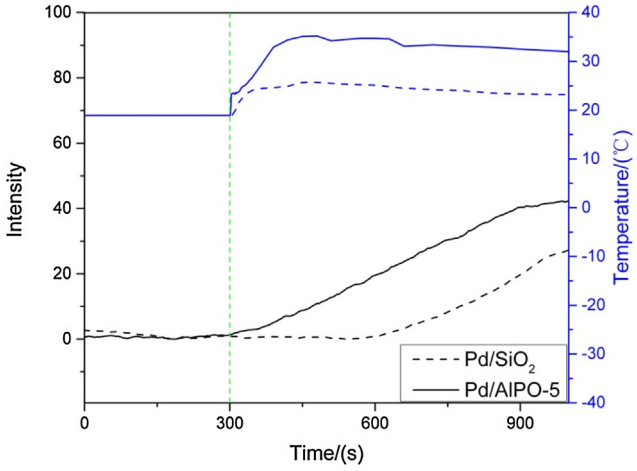

Fig. 4. TOF-MS analysis of tail gas during impregnation.

solution remain unchanged (Fig. 2). The pH value of the former impregnation solution decreases sharply to 4.5 and the latter is still 9.5. Fig. 3 shows the UV–vis spectra of the impregnated catalysts samples dried at 50 °C under vacuum. The bands centred at 250∼nm in both catalysts are assigned to charge transfer transition between the oxygen on the support and Pd according to previous report [27]. The band centred at 300 nm on Pd/SiO_2 belongs to the d → d transition characteristic of square planar complexes $[Pd(NH_3)_4]^{2+}$, which indicates that the $[Pd(NH_3)_4]^{2+}$ cations electrostatically adsorb on SiO_2. However, the spectrum of Pd/AlPO-5 shows a bathochromic and broadening band of d → d transition at 310 nm, which is near the band of $[Pd(NH_3)_3(H_2O)]^{2+}$ (317 nm) [28]. According to the distribution of $[Pd(NH_3)_{4-n}(H_2O)_n]^{2+}$ complexes in an aqueous solution with different pH value [29], it can be inferred that one of NH_3 ligands of Pd complex has been substituted. For Pd complex adsorbed on AlPO-5, NH_3 ligands may be substituted by Al-OH or P-OH (X-OH for short). The absorption band at 310 nm belongs to $[Pd(NH_3)_3(XOH)]^{2+}$. To test this idea, the tail gas during the impregnation of AlPO-5 was on-line analyzed by TOF-MS as large amounts of bubbles formed. The green dotted-line in Fig. 4 is the starting line of impregnation. NH_3 signal is detected immediately in the AlPO-5 impregnation system. Combined with the UV–vis result, it can be inferred that the released NH_3 come from the substituted NH_3 ligand. The temperature curve shows that the liquid temperature rises to 35 °C due to the water adsorption heat of AlPO-5 [30]. It has been reported that $[Pd(NH_3)_4]^{2+}$ complex would lose its ligand gradually after calcination, but the temperature is far beyond. For instance, Homeyer and Sachtler studied the pretreatment of $[Pd(NH_3)_4]^{2+}$ in zeolite NaY by TPMS. They found that the decomposition of $[Pd(NH_3)_4]^{2+}$ complex was a stepwise process: two of the NH_3 ligands were oxidized at 270 °C, another NH_3 was oxidized rapidly at 340 °C, and the last NH_3 ligand was oxidized at 400 °C [31,32]. Oxidation of the NH_3 ligands was found to yield N_2 and H_2O. In this research, the possibility of NH_3 ligand oxidation can be excluded since no N_2 signal is detected. The quick release of NH_3 in Pd/AlPO-5 system owes to the rapid substitution of NH_3 ligand by the surface X-OH groups to form $[Pd(NH_3)_3(XOH)]^{2+}$. The substitution benefits the formation of strong interaction between AlPO-5 support and $Pd(NH_3)_4(NO_3)_2$ precursor, which contributes to the suppression of Pd sintering. The tail gas of the SiO_2 impregnation system was also tested for comparison although no obvious bubbles were observed. Within first 300 s, no NH_3 signal is detected. The slowly emerged NH_3 signal attributes to excessive NH_3 dissolved in $Pd(NH_3)_4(NO_3)_2$ aqueous solution coming along with carrier gas.

The sintering of Rh nanoparticles supported on $AlPO_4$ has been reported to be significantly suppressed an Rh-O-P linkage at the interface between the metal and support [8,9]. Here it is speculated that the interaction between AlPO-5 support and $Pd(NH_3)_4(NO_3)_2$ precursor turn into Pd-O-P linkage after calcination, inhibiting the Pd sintering on Pd/AlPO-5 catalyst. Fig. 5a shows the spectra of unloaded AlPO-5 after being heated at elevated temperatures under He flow. AlPO-5 shows a very broad and strong absorption band cantered at approximately 3600 cm^{-1} at room temperature owing to its hydrophilicity. After water desorption, two bands appear at 3784 and 3668 cm^{-1} belonging to Al-OH and P-OH, respectively. The band of P-OH stretching is more intense than the band of Al-OH, which indicates that most of the surface groups of AlPO-5 are P-OH groups. Fig. 5b shows the DRIFT spectra of Pd/AlPO-5 with different Pd loadings. Two peaks of catalysts are located at the same position with the unsupported AlPO-5. But the intensity of P-OH peak decreases sharply with the increasing Pd loading while the intensity of Al-OH peak almost keeps constant. This can be considered that the X-OH groups involved in the NH_3 ligand substitution

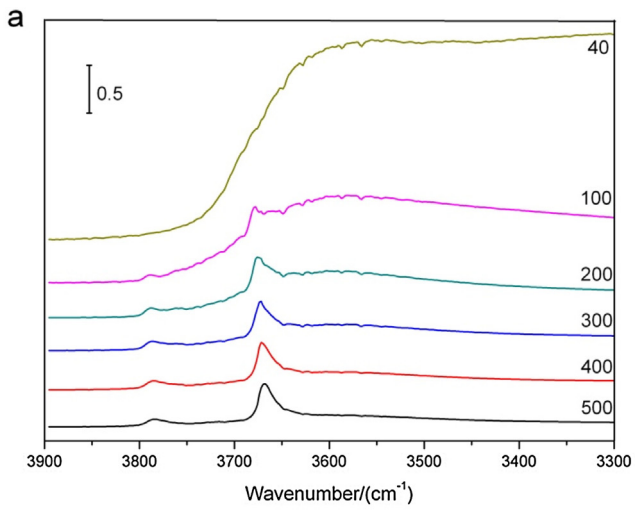

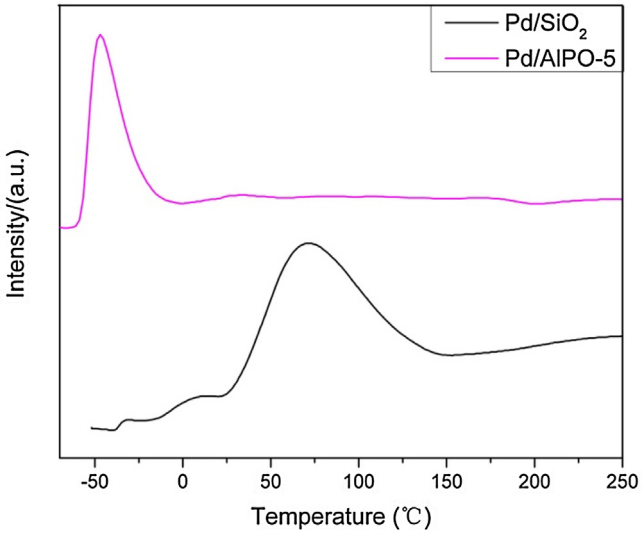

Fig. 6. H_2-TPR profile of Pd/AlPO-5 and Pd/SiO_2 catalysts.

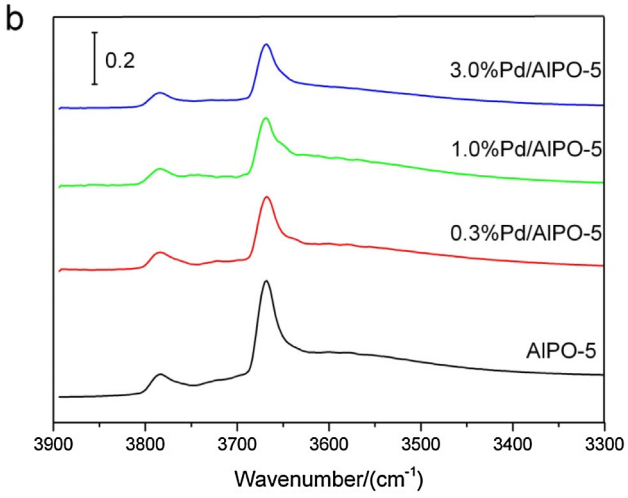

Fig. 5. (a) DRIFT spectra of AlPO-5 after dehydration at elevated temperatures under a He flow; (b) DRIFT spectra of Pd/AlPO-5 with different Pd loadings.

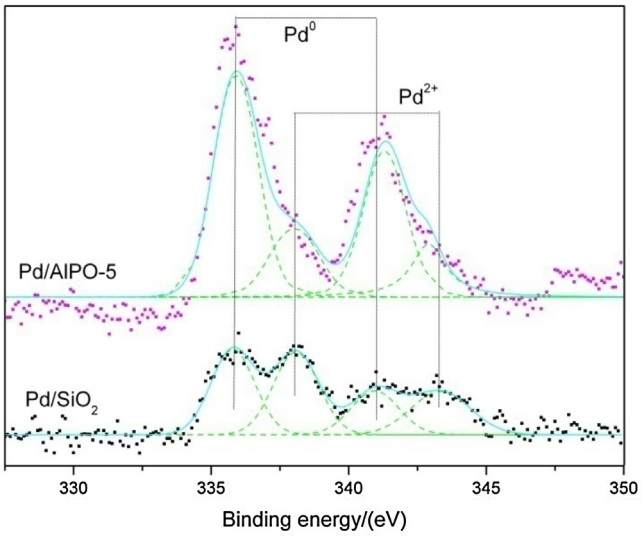

Fig. 7. Pd 3d XPS spectra of Pd/AlPO-5 and Pd/SiO_2 catalysts.

are P-OH to form $[Pd(NH_3)_3(POH)]^{2+}$, which benefit the formation of the Pd-O-P interfacial linkage. The Al-OH groups on the surface are not involved due to its low concentration.

H_2-temperature programmed reduction test was performed to characterize the reducibility of catalysts. In Fig. 6, it can be seen that PdO of Pd/AlPO-5 catalyst is reduced at −47 °C, while the centre of the broad Pd/SiO_2 reductive peak is located at 70 °C. Generally, reductive temperature difference is caused by different Pd particle size and Pd-support interaction. As shown in Fig. 1, the Pd particle size of Pd/AlPO-5 is smaller than that of Pd/SiO_2, which leads to the decreasing reduction temperature [33]. Also, the low reduction temperature is associated with the Pd-O-P interfacial linkage in Pd/AlPO-5 catalyst. According to previous report, the reduction temperature of Rh_2O_3 on Rh-$AlPO_4$ catalyst significantly decreased due to the formation of Rh-O-P linkage [34]. Different from the conventional electrostatic interactions at the metal-oxide support interface, the strong Rh-O-P linkage exists in both oxidizing and reducing atmosphere, leading to the decrease of reduction temperature. The lower reduction temperature of Pd supported on AlPO-5 further verified the formation of Pd-O-P interfacial linkage.

To further study the reducibility of the two catalysts, the electronic states of Pd supported on AlPO-5-and SiO_2 were determined by X-ray photoelectron spectrum (XPS) after pretreatment in H_2 at 70 °C. In Fig. 7, the two peaks at 335.9 eV and 341.0 eV can be assigned to Pd^0 $3d_{5/2}$ and Pd^0 $3d_{3/2}$, and the other two peaks at 338.0 eV as well as 343.2 eV belong to Pd^{2+} $3d_{5/2}$ and Pd^{2+} $3d_{3/2}$. For Pd/AlPO-5 catalyst, the areas of Pd^{2+} peaks take up a majority of the total peak area, which can be concluded that the PdO on Pd/AlPO-5 catalyst is almost reduced to metallic Pd after pretreatment. For Pd/SiO_2 catalyst, both Pd^0 and Pd^{2+} peaks with similar peak areas yield simultaneously under the same reduction condition, which indicate the reduction is not completed, even on the surface part. Hence, interaction between Pd and support is the critical reason for the reduction temperature change, rather than the Pd particle size. PdO supported on SiO_2 is not completely reduced after the pretreatment, which can be inferred that the reducibility of PdO supported on AlPO-5 is better than that on SiO_2. The reduction behaviour of PdO supported on AlPO-5 is affected by the formation of Pd-O-P interfacial linkage.

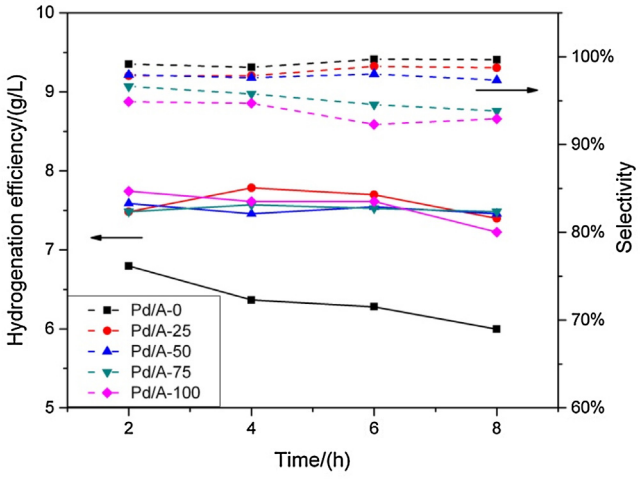

Fig. 8. Hydrogenation efficiencies and selectivities vs. reaction time over catalysts with different AlPO-5 content (Reaction conditions: T: 40 °C, absolute pressure: 0.4 Mpa, gas flow rate: 3 mL·min^{-1}, G/L: 10:1).

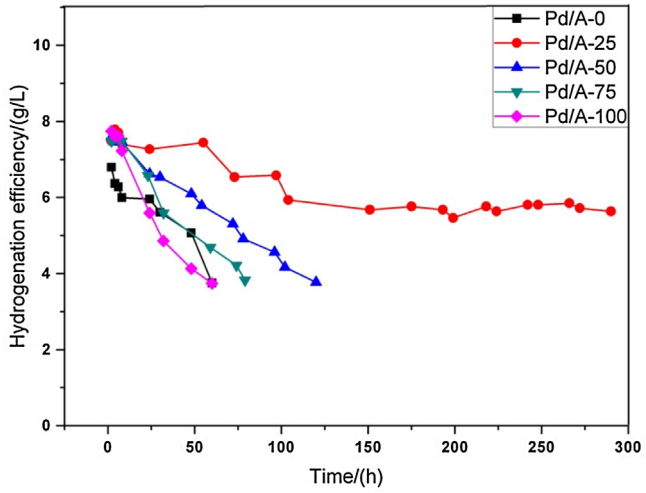

Fig. 9. Hydrogenation efficiency vs. reaction time over Pd catalysts (Reaction conditions: T: 40 °C, absolute pressure: 0.4 Mpa, gas flow rate: 3 mL·min^{-1}, G/L: 10:1).

3.2. Catalyst performance

Apart from Pd/AlPO-5 and Pd/SiO2 catalysts, three catalysts supported on SiO_2-AlPO-5 composite with different AlPO-5 content were prepared and tested for the hydrogenation of 2-ethylanthraquinone. All catalysts are named after AlPO-5 content (Pd/AlPO-5: Pd/A-100, Pd/25%-SiO_2-75%AlPO-5: Pd/A-75, Pd/50%-SiO_2-50%AlPO-5: Pd/A-50, Pd/75%-SiO_2-25%AlPO-5: Pd/A-25, Pd/SiO2: Pd/A-0) (Table 1). Fig. 8 exhibits the time dependences of hydrogenation efficiency (H_2O_2 yield) and active quinone selectivity in a continuous trickle bed reactor at 40 °C. The detailed selectivity data is shown in Table S1. The reaction condition is set to control hydrogenation degree to simulate the situation of H_2O_2 industrial production. It can be seen that the Pd/A-0 sample exhibits the lowest hydrogenation efficiency and the highest active quinone selectivity. After AlPO-5 added, the hydrogenation efficiencies increase obviously. Similar to Pd/A-100, catalyst containing AlPO-5 has high Pd dispersion and good reducibility (Table 1, Figs. S3–S5). However, the active quinone selectivities decrease with the amount of AlPO-5. Catalysts containing AlPO-5 achieve higher initial hydrogenation efficiency attributed to higher Pd dispersion. With increasing AlPO-5 content, both of the specific surface area and pore volume decrease (Table 1). Moreover, the ratio of small pore increases sharply with increasing AlPO-5 content, which limit the mass transfer of AQ molecule and AQH_2 molecule (Fig. S6). The prolonged residence time may lead to the formation of by-products from deep hydrogenation. With increasing amount of AlPO-5, the active quinone selectivity decrease and the catalysts tend to deactivate more quickly. As shown in Fig. 9, the Pd/A-25 sample achieves stable hydrogenation efficiency about 6 g·L^{-1} H_2O_2 in 300 h stability test. Catalysts with more AlPO-5 in support deactivate quickly, especially Pd/A-100 sample. Meanwhile, the Pd/A-0 sample exhibits lower initial hydrogenation efficiency as well as poor stability. Because of lower Pd dispersion, the number of active site of Pd/A-0 catalyst is less. Moreover, as a three phase reaction, there is a thin liquid film on the surface of catalyst, which may inhibit H_2 transferring to surface active sites. It is disadvantageous for H_2 dissociation to provide active species, which leads to lower initial hydrogenation efficiency and decreasing hydrogenation efficiency. Because of lower Pd dispersion, the number of active site of Pd/A-0 catalyst is less than other catalysts. Hence, the detrimental effect on hydrogenation efficiency is more significant on Pd/A-0 catalyst. Therefore, Pd/A-0 catalyst deactivates quickly although it achieve high selectivity. Pd/A-25 shows better performance with a suitable ratio of AlPO-5 to keep the balance of activity and selectivity. It is expected to decrease precious metal content in industrial application. Furthermore, the hydrogenation efficiency of Pd/A-25 catalyst was also compared with commercial catalyst and literature data. As seen in Fig. S5, Pd/A-25 catalyst achieved higher activity than other two catalysts, suggesting that AlPO-5 is a competitive choice for catalyst support.

4. Conclusions

Highly dispersed Pd/AlPO-5 catalyst was prepared by impregnation method and tested in the hydrogenation of 2-ethylanthraquinone. Characterization results suggested that the abundant surface P-OH groups substituted the NH_3 ligand of $[Pd(NH_3)_4]^{2+}$ precursor to form $[Pd(NH_3)_3(POH)]^{2+}$. After calcination, the latter formed Pd-O-P interfacial linkage between Pd nanoparticles and AlPO-5, benefiting the suppression of Pd sintering. Catalyst supported on SiO_2-AlPO-5 composite (25% AlPO-5) exhibited improved catalytic activity and stability in consideration of the mass transfer of reactant molecules, which is expected to decrease precious metal content in industrial application.

Acknowledgement

This work was supported by the National Natural Science Foundation of China (21306184).

Appendix A. Supplementary data

Supplementary data associated with this article can be found, in the online version, at http://dx.doi.org/10.1016/j.apcata.2016.10.007.

References

[1] A.T. Bell, Science 299 (2003) 1688–1691.
[2] S.J. Tauster, S.C. Fung, J. Catal. 55 (1978) 29–35.
[3] S.J. Tauster, S.C. Fung, R.L. Garten, J. Am. Chem. Soc. 100 (1978) 170–175.
[4] Y. Nagai, K. Dohmae, Y. Ikeda, N. Takagi, T. Tanabe, N. Hara, G. Guilera, S. Pascarelli, M.A. Newton, O. Kuno, H.Y. Jiang, H. Shinjoh, S. Matsumoto, Angew. Chem. Int. Ed. 47 (2008) 9303–9306.
[5] J.H. Kwak, J. Hu, D. Mei, C.-W. Yi, D.H. Kim, C.H.F. Peden, L.F. Allard, J. Szanyi, Science 325 (2009) 1670–1673.
[6] Y. Nagai, T. Hirabayashi, K. Dohmae, N. Takagi, T. Minami, H. Shinjoh, S. Matsumoto, J. Catal. 242 (2006) 103–109.
[7] H. Tang, J. Wei, F. Liu, B. Qiao, X. Pan, L. Li, J. Liu, J. Wang, T. Zhang, J. Am. Chem. Soc. 138 (2016) 56–59.

[8] M. Machida, K. Murakami, S. Hinokuma, K. Uemura, K. Ikeue, M. Matsuda, M. Chai, Y. Nakahara, T. Sato, Chem. Mater. 21 (2009) 1796–1798.
[9] M. Machida, S. Minami, K. Ikeue, S. Hinokuma, Y. Nagao, T. Sato, Y. Nakahara, Chem. Mater. 26 (2014) 5799–5805.
[10] E. Santacesaria, M. Di Serio, A. Russo, U. Leone, R. Velotti, Chem. Eng. Sci. 54 (1999) 2799–2806.
[11] J.M. Campos-Martin, G. Blanco-Brieva, J.L.G. Fierro, Angew. Chem. Int. Ed. 45 (2006) 6962–6984.
[12] C. Samanta, Appl. Catal. A: Gen. 350 (2008) 133–149.
[13] T. Kamachi, T. Ogata, E. Mori, K. Iura, N. Okuda, M. Nagata, K. Yoshizawa, J. Phys. Chem. C 119 (2015) 8748–8754.
[14] A. Drelinkiewicz, A. Waksmundzka-Gora, W. Makowski, J. Stejskal, Catal. Commun. 6 (2005) 347–356.
[15] K.H. Meyer, Liebigs Ann. Chem. 379 (1911) 37–78.
[16] X. Li, H. Su, G. Ren, S. Wang, RSC Adv. 5 (2015) 100968–100977.
[17] C. Shen, Y.J. Wang, J.H. Xu, Y.C. Lu, G.S. Luo, Chem. Eng. J. 173 (2011) 226–232.
[18] R. Kosydar, A. Drelinkiewicz, J.P. Ganhy, Catal. Lett. 139 (2010) 105–113.
[19] P. Gallezot, D. Richard, Cat. Rev.— Sci. Eng. 40 (1998) 81–126.
[20] A. Drelinkiewicz, R. Kangas, R. Laitinen, A. Pukkinen, J. Pursiainen, Appl. Catal. A: Gen. 263 (2004) 71–82.
[21] A. Drelinkiewicz, A. Pukkinen, R. Kangas, R. Laitinen, Catal. Lett. 94 (2004) 157–170.
[22] R. Kosydar, A. Drelinkiewicz, E. Lalik, J. Gurgul, Appl. Catal. A: Gen. 402 (2011) 121–131.
[23] A. Drelinkiewicz, A. Waksmundzka-Góra, J. Mol. Catal. A: Chem. 258 (2006) 1–9.
[24] C. Wang, L. Wang, J. Zhang, H. Wang, J.P. Lewis, F.-S. Xiao, J. Am. Chem. Soc. 138 (2016) 7880–7883.
[25] L. Wang, J. Zhang, X. Yi, A. Zheng, F. Deng, C. Chen, Y. Ji, F. Liu, X. Meng, F.S. Xiao, ACS Catal. 5 (2015) 2727–2734.
[26] S.T. Wilson, B.M. Lok, C.A. Messina, T.R. Cannan, E.M. Flanigen, J. Am. Chem. Soc. 104 (1982) 1146–1147.
[27] Z. Zhang, G. Mestl, H. Knözinger, W. Sachtler, Appl. Catal. A: Gen. 89 (1992) 155–168.
[28] L. Bonneviot, O. Legendre, M. Kermarec, D. Olivier, M. Che, J. Colloid Interface Sci. 134 (1990) 534–547.
[29] D. Spielbauer, H. Zeilinger, H. Knoezinger, Langmuir 9 (1993) 460–466.
[30] Y.I. Aristov, J. Chem. Eng. Jpn. 40 (2007) 1242–1251.
[31] S. Homeyer, W. Sachtler, J. Catal. 117 (1989) 91–101.
[32] S. Homeyer, W. Sachtler, Appl. Catal. 54 (1989) 189–202.
[33] M. Gurrath, T. Kuretzky, H.P. Boehm, L.B. Okhlopkova, A.S. Lisitsyn, V.A. Likholobov, Carbon 38 (2000) 1241–1255.
[34] M. Machida, S. Minami, S. Hinokuma, H. Yoshida, Y. Nagao, T. Sato, Y. Nakahara, J. Phys. Chem. C 119 (2015) 373–380.